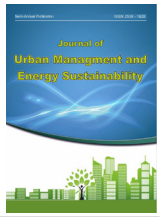
Int. J. Urban Manage Energy Sustainability, 7(2): 449-468, 2026

International Journal of Urban Management and Energy Sustainability (IJUMES)

Homepage: http://www.ijumes.com



ORIGINAL RESEARCH PAPER

A Microstretch Mixture Theory for Differential Land Subsidence and Earth-Fissure Initiation from Non-uniform Aquifer Drawdown

Amir Ghiasi Tarzi, Amir Robati*, Mohammad Ali Kazerooni Sadi

Department of Civil Engineering, Ke.C., Islamic Azad university, Kerman, Iran

ARTICLE INFO

Article History:
Received 2026-02-11
Revised 2026-04-10
Accepted 2026-05-25

Keywords:
Cosserat length scale; earth fissures; microstretch continuum; principle of virtual power; theory of Porous media

ABSTRACT

Groundwater pumping lowers aquifer heads unevenly, and where the resulting land subsidence varies laterally it opens damaging earth fissures. Classical poroelasticity treats the soil skeleton as a structureless Cauchy continuum, predicts a sharp horizontal-strain concentration at the margin of the subsidence bowl, and has no intrinsic length scale to set the width of the fissure zone, whereas existing Cosserat descriptions of the skeleton omit the pore fluid. This study develops a microstretch mixture theory for saturated porous media in which the solid skeleton carries grain-scale rotation and dilatation coupled two-way to a non-polar pore fluid. The balance laws are derived from the principle of virtual power and closed by the Coleman–Noll procedure within the Theory of Porous Media, and the linearized theory is applied to the plane-strain consolidation of an aquitard under laterally varying drawdown. The theory introduces two internal length scales. Its Cosserat length caps the peak horizontal tensile strain and spreads it over a fissure zone of finite width, depending on its ratio to the layer thickness: at grain and shear-band scales the classical Biot prediction is recovered, whereas a structural length that is a sizeable fraction of the layer thickness reduces the peak to about seven-tenths of the classical value. The fissure-driving strain is largest early in consolidation, shortly after the head decline. For uniform drawdown the theory reduces exactly to the microdilatational-mixture and Biot–Terzaghi limits. The framework unifies tension- and rotation-based accounts of earth fissuring and yields testable predictions of fissure width, intensity, and timing.

DOI: 10.22034/ijumes.2026.2110389.1432

Running Title: Theory for Differential Land Subsidence and Earth-Fissure Initiation

NUMBER OF REFERENCES	NUMBER OF FIGURES	NUMBER OF TABLES
40	02	01

*Corresponding Author:
Email: *Ammirrr@yahoo.com*
Phone: 00983433210043
ORCID: https://orcid.org/0000-0001-5086-5932

INTRODUCTION

Groundwater withdrawal is among the most widespread causes of land subsidence (Galloway & Burbey, 2011; Poland, 1984). Where the pumping-induced head decline varies laterally (across the edge of a well field, a basin margin, or a buried bedrock step), the bounding aquitards compact by differing amounts, the land surface subsides into a bowl, and horizontal ground strains develop. Where those strains are tensile they open earth fissures: linear tension cracks that damage foundations, canals, and transport infrastructure across the subsiding basins of the US Southwest, the North China Plain, and elsewhere (Holzer & Pampeyan, 1981; Wang et al., 2025; Ye et al., 2018). Classical poroelasticity, built on a structureless Cauchy skeleton, predicts a sharp concentration of horizontal strain at the bowl margin and gives no intrinsic length scale to set the width of the fissure zone; and although a Cosserat (micropolar) description of the dry skeleton has been advanced for this problem (Budhu, 2011; Budhu & Adiyaman, 2010), it omits the pore fluid whose evolution drives the compaction. This paper supplies the missing element: a saturated generalized-continuum mixture in which grain-scale rotation and dilatation are coupled two-way to the pore fluid.

The skeleton of a real soil has structure below the continuum point: it is a packing of grains that, as it is loaded and as pore fluid passes through it, can both rotate and rearrange, altering the local pore geometry. Classical poroelasticity ignores this microstructure altogether; micropolar mixture theories admit grain rotation but not grain-scale volume change. To carry both, we develop a microstretch mixture theory: a saturated binary mixture of a microstretch solid skeleton (whose grains may rotate and dilate) and a non-polar elastic pore fluid. Both microstructural degrees of freedom matter here: the rotation sector, activated wherever the compaction varies laterally, regularizes the horizontal strain that opens fissures by an amount set by its internal length scale, while the grain-scale dilatation carries the volumetric coupling to the pore fluid. Together they determine how the width, intensity, and timing of the fissure zone depart from the classical prediction, which carries no length scale of its own.

Two established extensions of continuum mechanics are brought together (Bedford & Drumheller, 1983; Maugin, 2017). In mixture theory (Atkin & Craine, 1976; Truesdell, 1984) the skeleton and the fluid occupy the same region as superposed continua, each with its own motion and its own balance laws, and exchange momentum through interaction supplies. Micromorphic theory (Eringen, 1999) endows each material point with microstructural degrees of freedom; its microstretch restriction, obtained by limiting the micro-deformation to a rotation composed with an isotropic dilatation, $\chi = R_{\chi} \cdot (\beta 1)$, is the minimal kinematics carrying both grain rotation and grain dilatation while remaining far simpler than the full micromorphic continuum. It is thus the natural model for a granular skeleton whose grains can simultaneously rotate and swell. The pore fluid carries no orientational or dilatational microstructure of its own at the continuum scale and is therefore modeled as a simple non-polar fluid: giving it microstructure would add material constants without a physical counterpart, together with interaction supplies that the non-polar choice eliminates from the start. The balance laws of a generalized continuum can be constructed along several systematic routes (dell'Isola & Placidi, 2011; Del Piero, 2009; Green & Rivlin, 1964; Mariano, 2016; Noll, 1974). Here they are obtained from the principle of virtual power (Germain, 1973, 2020): one statement about the power expended by internal and external actions yields the field equations together with their natural boundary conditions, and it accommodates the microstructural fields on the same footing as the displacement. Constitutive closure follows the Coleman–Noll procedure (Coleman & Noll, 1974; Hütter, 2020) in the setting of the Theory of Porous Media (Diebels, 2001; Ehlers, 2002; Hassanizadeh & Gray, 1979a, 1979b), with

the volume fraction entering as an internal state variable. Since the mineral grains of a saturated soil are practically incompressible, the porosity is tied kinematically to the skeleton dilatation rather than being an independent energetic variable; the grain-scale structural response resides in the microstretch, and the porosity energetics is counted once.

The two ingredients have been developed separately (micropolar solid–fluid mixtures within the Theory of Porous Media (Diebels & Ehlers, 1996), the more general micromorphic mixture theory of Twiss and Eringen (1971), and the single-constituent microstretch continuum by Eringen (1999)), but their combination for a saturated solid–fluid medium has not. The nearest precedent is the work of Chiriță and Galeș (2008) on a mixture of two microstretch solids, aimed at viscoelastic composites. Three differences, each consequential for a saturated porous medium, separate the present theory from it: the second constituent is a non-polar fluid rather than a second microstretch solid, so that the angular- and microstretch-momentum interaction supplies drop out; the volume fraction obeys the TPM saturation constraint instead of a Lagrangian two-solid description; and the balance laws are derived from virtual power rather than postulated, so that their boundary conditions and the admissible interaction terms emerge together. In the appropriate limits the framework reduces to the micropolar- and microdilatation-mixture theories and to classical Biot–Terzaghi poroelasticity.

The contribution is a thermodynamically consistent generalized-continuum theory of saturated porous media, derived from the principle of virtual power, in which the solid skeleton carries grain-scale rotation and dilatation coupled two-way to a non-polar pore fluid. Applied to the differential compaction of an aquitard under laterally-varying drawdown (a loading that activates both microstructural sectors), the theory introduces two internal length scales and predicts that a Cosserat length scale of the skeleton regularizes the earth-fissure zone: it caps the peak horizontal tensile strain and turns the sharp classical strain concentration into a finite zone that broadens with the Cosserat length, by an amount set by the ratio of that length to the layer thickness, while the fissure-driving strain develops in time and is largest early in the consolidation. When the drawdown is spatially uniform the rotation sector switches off and the theory reduces exactly to the microdilatational-mixture limit (Section 4.4) and to classical Biot–Terzaghi poroelasticity. These predictions (the finite fissure-zone width, the reduced peak strain, and the timing of maximum fissure risk) carry the theory's testable content and bring the tension- and rotation-based descriptions of earth fissuring together in a single fluid-coupled model.

The paper is organized as follows. Section 2 recalls the non-polar binary mixture that serves as the classical reference, its linearization being collected in Appendix A. Section 3 develops the single-constituent microstretch continuum (linearization in Appendix B), and Section 4 combines the two into the microstretch mixture theory, verifying the micropolar and microdilatation limits (linearization in Appendix C). Section 5 applies the linearized theory to differential land subsidence and earth-fissure initiation under non-uniform aquifer drawdown, and Section 6 concludes. Notation: vectors are lower-case bold and second-order tensors upper-case bold; a superposed dot denotes the material time derivative; the constituent label $\alpha\in\{s,f\}$ is written as a superscript (α), with no summation over it unless stated.

MATERIALS AND METHODS

Continuum mixture theory

This section establishes the two-constituent poroelastic baseline of the theory. It is deliberately standard (a non-polar solid skeleton saturated by a pore fluid) so that the microstructural effects introduced from Section 3 onward are cleanly attributable to the microstretch kinematics

rather than to the mixture description itself. The balance laws and effective-stress structure recovered here are those of the classical Theory of Porous Media (Atkin & Craine, 1976; Bowen, 1976; Ehlers, 2002; Truesdell, 1984); we recapitulate them compactly via the principle of virtual power, both to fix notation and because the same variational argument carries unchanged into the microstretch mixture of Section 4. Throughout, superscripts (s) and (f) label the solid and fluid constituents; the principal symbols are collected in (Tab. 1).

Table 1: Principal notation.

Symbol	Meaning
$\phi^{(\alpha)}$, $X^{(\alpha)}$	motion of constituent ; reference (material) position
$n^{(\alpha)}$	volume fraction of constituent α ($n^{(s)}+n^{(f)}=1$)
$\rho^{(\alpha)}$, $\rho^{R(\alpha)}$	partial and real (intrinsic) mass density
$v^{(\alpha)}$, $v^{(fs)}$	constituent velocity; seepage velocity $v^{(f)}-v^{(s)}$
$u^{(\alpha)}$	displacement of constituent α
grad, div	spatial gradient and divergence (w.r.t. x)
Grad, Div	referential gradient and divergence (w.r.t. X)
ϵ	third-order permutation (Levi–Civita) tensor
$F^{(s)}$, $C^{(s)}$	solid deformation gradient; right Cauchy–Green tensor
$\chi^{(s)}$, $R_\chi^{(s)}$	solid micro-deformation; micro-rotation tensor
$\beta^{(s)}$, $\varphi^{(s)}$	scalar microstretch ratio; perturbation $\beta^{(s)}$-1
$\upsilon^{(s)}$, $\Omega^{(s)}$, $\omega^{(s)}$	micro-gyration; micro-rotation rate; its axial vector
$\vartheta^{(s)}$, Θ	plane-strain micro-rotation angle (Section 5); macro-rotation angle $1/2\,(\partial_z u_x^{(s)} - \partial_x u_z^{(s)})$
$\varepsilon^{(s)}$, $e_1^{(s)}$	linear microstretch strain; microstretch dilatation
$\Gamma_{(s)}$, $K^{(s)}$	micro-curvature; micro-dilatation gradient
$T^{(\alpha)}$, $M^{(s)}$	partial (force) stress; couple stress
$s^{(s)}$, $m^{(s)}$	scalar microstretch stress; microstretch double-stress
$t^{(\alpha)}$, n	partial traction vector; outward unit normal
$pl^{(\alpha)}$	momentum supply (interaction force)
$b_0^{(\alpha)}$, l_c, l_d	body force; body couple; microstretch body action
$\psi^{(\alpha)}$, $D^{(\alpha)}$	Helmholtz free energy; rate of deformation
p_{th}, B	thermodynamic pore pressure; drag tensor
$\lambda^{(s)}$,$\mu^{(s)}$, $\kappa^{(s)}$	drained Lamé moduli; Cosserat shear modulus
$a^{(s)}$,$b^{(s)}$,$c_1^{(s)}$	microstretch moduli and length-scale modulus
$\omega^{(s)}$, τ_φ	equilibrated-force dissipation coefficient; microdilatation relaxation time $\omega^{(s)}/9a^{(s)}$
$\alpha_1^{(s)}$,$\alpha_2^{(s)}$,$\alpha_3^{(s)}$	isotropic curvature (couple-stress) moduli
κ_f, k	fluid bulk modulus; hydraulic mobility ($k=K_v/\gamma_w$)
K_v, γ_w	vertical hydraulic conductivity; unit weight of water
c_v, l_c, l_v, q	consolidation coefficient; Cosserat and microdilatation lengths; lateral wavenumber
h, Δp_0, S	aquitard thickness; head-decline pressure; subsidence

Kinematics and mass balance

The mixture is represented by two superimposed continua (a solid and a fluid constituent) occupying the three-dimensional differentiable

manifolds $B^{(s)}$ and $B^{(f)}$. Each constituent is carried by its own smooth, invertible motion,

$$x=\phi^{(\alpha)}(X^{(\alpha)},t),\quad \alpha\in\{s,f\}. \tag{1}$$

Here $\phi^{(\alpha)}$ is the motion (deformation map) of constituent α, $X^{(\alpha)}$ its reference (material) position, and x the current spatial position. The basic postulate of mixture theory, due to Truesdell (1984), is that each spatial point x is simultaneously occupied by both constituents. The partial density $\rho^{(\alpha)}$ and real density $\rho^{R}(\alpha)$ are related by

$$\rho^{(\alpha)}=n^{(\alpha)}\rho^{R(\alpha)}, \tag{2}$$

in which the volume fraction $n^{(\alpha)}$ enters as an internal state variable (Hassanizadeh & Gray, 1979a, 1979b). Full saturation of the binary mixture then requires

$$n^{(s)}+n^{(f)}=1. \tag{3}$$

The constituent velocity and the material time derivative following α are

$$\mathbf{v}^{(\alpha)}=\frac{\partial\boldsymbol{\phi}^{(\alpha)}}{\partial t}\qquad \frac{d^{(\alpha)}A}{dt}=\frac{\partial A}{\partial t}+\mathrm{grad}A\cdot\mathbf{v}^{(\alpha)}, \tag{4}$$

Here $v^{(\alpha)}$ is the constituent velocity, $d^{(\alpha)}/dt$ the material time derivative following constituent α, and grad the spatial gradient (with respect to x). In the absence of mass exchange between constituents, conservation of mass holds separately for each constituent with local form

$$\frac{d^{(\alpha)}\rho^{(\alpha)}}{dt}+\rho^{(\alpha)}\,\mathrm{div}\mathbf{v}^{(\alpha)}=0, \tag{5}$$

Here div denotes the spatial divergence (with respect to x).

Virtual power and balance laws

Each non-polar constituent α is endowed with an internal virtual power

$$P_i^{(\alpha)}=\int_{\mathcal{P}^{(\alpha)}}\mathbf{T}^{(\alpha)}:\mathbf{L}^{*}_{(\alpha)}\,dv \tag{6}$$

in which $P^{(\alpha)}$ is the current spatial region occupied by α, $T^{(\alpha)}$ its partial (Cauchy) stress, and $L_{(\alpha)}^{*}$ the gradient of the constituent's virtual velocity. Objectivity of (6) renders each $T^{(\alpha)}$ symmetric (the non-polar assumption, consistent with (Atkin & Craine, 1976)). Since the treatment is quasi-static throughout (Section 5), inertia is discarded in full (kinetic-energy and acceleration terms are absent), and the balance laws retain only the ordinary body force $b_0^{(\alpha)}$. The divergence theorem, applied together with the balance of internal and external virtual power, then delivers the linear-momentum balance and its traction condition,

$$\mathrm{div}T^{(\alpha)}+b_0^{(\alpha)}+pl^{(\alpha)}\&=0 \tag{7}$$

$$t^{(\alpha)}=T^{(\alpha)}\cdot n \tag{8}$$

with $t^{(\alpha)}$ the partial traction on constituent α, n the outward unit surface normal, and $pl^{(\alpha)}$ the momentum supplied by the companion constituent. Invariance of the total mixture virtual power (Quiligotti et al., 2003) then demands

$$pl^{(s)}+pl^{(f)}=0, \tag{9}$$

the momentum balance for the mixture as a whole; the balance of angular momentum holds identically owing to the symmetry of each $T^{(\alpha)}$.

Free-energy inequality and constitutive equations

Using (9) to consolidate the interaction terms, the mixture free-energy inequality (Atkin & Craine, 1976) takes the form

$$\rho^{(s)}\frac{d^{(s)}\psi^{(s)}}{dt}+\rho^{(f)}\frac{d^{(f)}\psi^{(f)}}{dt}-\mathbf{T}^{(s)}:\mathbf{D}^{(s)}-\mathbf{T}^{(f)}:\mathbf{D}^{(f)}+\mathbf{pl}^{(f)}\cdot\mathbf{v}^{(fs)}\ \le\ 0 \tag{10}$$

Here $\psi^{(\alpha)}$ denotes the Helmholtz free energy per unit mass of α, $D^{(\alpha)}$ the constituent rate of deformation (the symmetric part of the spatial velocity gradient), and $v^{(fs)}=v^{(f)}-v^{(s)}$ the seepage

velocity. Closure follows from the Coleman–Noll procedure (Coleman & Noll, 1974; Hütter, 2020), for which we posit the free energies

$$\psi^{(s)}=\psi^{(s)}(C^{(s)}),\ \psi^{(f)}=\psi^{(f)}(\rho^{R(f)}), \tag{11}$$

with $F^{(s)}$ the solid deformation gradient and $C^{(s)}=(F^{(s)})^{T}\cdot F^{(s)}$ its right Cauchy–Green tensor. The skeleton is hyperelastic, storing energy through deformation alone, whereas the pore fluid is barotropic and inviscid, its energy fixed solely by the real density $\rho^{R(f)}$. Following usual practice for water-saturated soils and aquitards (Ehlers, 2002), the mineral grains are treated as materially incompressible ($\rho^{R(s)}$ =const); the solid mass balance $d^{(s)}\rho^{(s)}/dt+\rho^{(s)}\,\mathrm{div}v^{(s)}=0$ thereupon collapses to

$$\frac{d^{(s)}n^{(s)}}{dt}=-n^{(s)}\,\mathrm{div}\mathbf{v}^{(s)} \tag{12}$$

so that the porosity is slaved to the skeleton dilatation. The solid volume fraction $n^{(s)}$ therefore enters only as a kinematic variable, not as an independent energetic degree of freedom; the grain-scale structural response is instead carried by the microstretch of Section 4, so the porosity energetics is not double-counted.

Solid constitutive equation.

Inserting (11) into (10) and invoking the Coleman–Noll argument gives the solid partial stress

$$\mathbf{T}^{(s)}=2\rho^{(s)}\mathbf{F}^{(s)}\cdot\frac{\partial\psi^{(s)}}{\partial\mathbf{C}^{(s)}}\cdot\left(\mathbf{F}^{(s)}\right)^{T}-p_{th}\,n^{(s)}\,\mathbf{1} \tag{13}$$

in which the thermodynamic (real-fluid) pressure is defined by

$$p_{th}:=\frac{\rho^{(f)}}{n^{(f)}}\,\rho^{R(f)}\frac{\partial\psi^{(f)}}{\partial\rho^{R(f)}}=(\rho^{R(f)})^{2}\frac{\partial\psi^{(f)}}{\partial\rho^{R(f)}} \tag{14}$$

where $\rho^{(f)}/n^{(f)}=\rho^{R(f)}$ has been used. The leading term of (13) is the drained hyperelastic skeleton stress, and $-p_{th}n^{(s)}1$ is the Biot–Terzaghi pore-pressure coupling; because $\psi^{(s)}$ carries no dependence on $n^{(s)}$, no configurational pressure appears.

Fluid constitutive equations.

With the fluid inviscid ($\psi^{(f)}$ being independent of the fluid rate of deformation $D^{(f)}$), the Coleman–Noll procedure returns a fluid stress that is pure pressure,

$$T^{(f)}=-n^{(f)}p_{th}1 \tag{15}$$

and the momentum supply separates into an equilibrium (buoyancy) contribution and a dissipative Darcy drag,

$$pl^{(f)Eq}=p_{th}\,\mathrm{gradn}^{(f)}=-p_{th}\,\mathrm{gradn}^{(s)} \tag{16}$$

$$pl^{(f)NEq}=-B\cdot v^{(fs)} \tag{17}$$

in which B is a positive semi-definite drag tensor signed after the convention of Diebels (2001) and Ehlers (2002), so that the drag resists relative seepage $v^{(fs)}=v^{(f)}-v^{(s)}$. The equilibrium part (16) is the Theory-of-Porous-Media buoyancy term of Ehlers (2002): it cancels the volume-fraction-gradient contribution $-p_{th}\mathrm{gradn}^{(f)}$ of $\mathrm{divT}^{(f)}$, so that the fluid momentum balance reduces to Darcy's law $-n^{(f)}\,\mathrm{gradp}_{th}=B\cdot v^{(fs)}$ (it vanishes identically in the linearized, uniform-n_0 setting of Section 5). Viscosity therefore acts only through the Darcy drag coefficient in (17) and not as a bulk fluid stress; the residual inequality $B\cdot v^{(fs)}\otimes v^{\wedge(fs)}\geq 0$ is met by the semi-definiteness of B.

In the small-strain, isotropic limit these relations specialize to the linear Biot–Terzaghi constitutive equations. Expanding about the natural reference state (where the solid infinitesimal strain is $\varepsilon^{(s)}=1/2\,(\mathrm{Gradu}^{(s)}+(\mathrm{Gradu}^{(s)})^{T})$ and the pre-stress $-[p_{th}]_0\,n_0^{(s)}1$ drops out), the solid partial stress, the pore pressure, the fluid partial stress, and the seepage law become

$$\mathbf{T}^{(s)}=\lambda^{(s)}\left(\mathrm{tr}\boldsymbol{\varepsilon}^{(s)}\right)\mathbf{1}+2\mu^{(s)}\boldsymbol{\varepsilon}^{(s)}-n_0^{(s)}p_{th}\,\mathbf{1} \tag{18}$$

$$p_{th}=-\kappa_f\,\mathrm{Div}\mathbf{u}^{(f)} \tag{19}$$

$$\mathbf{T}^{(f)}=-n_0^{(f)}p_{th}\,\mathbf{1} \tag{20}$$

$$\mathbf{pl}^{(f)}=-\frac{1}{k}\,\mathbf{v}^{(fs)} \tag{21}$$

where $u^{(\alpha)}$ is the displacement of constituent α; Grad and Div are the referential gradient and divergence (with respect to X), which coincide with the spatial operators grad, div in the small-deformation regime adopted here; $\lambda^{(s)}$,$\mu^{(s)}$ are the drained Lamé constants, κ_f the fluid bulk modulus, $n_0^{(s)}$ the reference solid volume fraction, and k the hydraulic mobility ($k=K_v/\gamma_w$, with K_v the vertical hydraulic conductivity and γ_w the unit weight of water). Equations (18)–(21) are the linear Biot–Terzaghi poroelasticity equations (Biot, 1941; Terzaghi, 1943): an effective-stress relation with total coefficient $n_0^{(s)} + n_0^{(f)} = 1$, a fluid storage relation, and Darcy's law. That the Theory of Porous Media reduces in this linear limit to Biot's equations is well established (Bowen, 1980, 1982; Ehlers, 2002). No configurational pressure, volume-fraction stiffness, or bulk fluid viscosity appears here: the grain-scale structural response is deferred to the microstretch of Section 4. The full derivation is given in Appendix A.

Microstretch continuum

Independently of the mixture, this section develops the microstretch continuum, the single-constituent building block that endows a material point with grain-scale rotational and dilatational degrees of freedom. The continuum and its field equations are due to Eringen (1999), in the micromorphic lineage of Mindlin (1964); we re-derive them from the principle of virtual power (Germain, 1973, 2020) so that the single-constituent results pass directly into the mixture of Section 4. It is combined with the mixture framework of Section 2 in Section 4.

Kinematics of the microstretch continuum

The kinematics of a micromorphic-type continuum is described by the macroscopic motion ϕ and a micro-deformation tensor χ that maps a triad of reference directors Ξ_i into their deformed counterparts $\xi_i = \chi \cdot \Xi_i$. The polar decomposition $\chi = R_\chi \cdot U_\chi$ defines the micro-rotation tensor R_χ and the right micro-stretch tensor U_χ. Different restrictions on χ generate the standard hierarchy:

$$\begin{aligned}
\boldsymbol{\chi} &= \mathbf{1} \cdot \mathbf{U}_\chi && \rightarrow \text{microstrain continuum,}\\
\boldsymbol{\chi} &= \mathbf{R}_\chi \cdot (\beta \mathbf{1}) && \rightarrow \text{microstretch continuum,}\\
\boldsymbol{\chi} &= \mathbf{R}_\chi \cdot \mathbf{1} && \rightarrow \text{micropolar continuum,}\\
\boldsymbol{\chi} &= \mathbf{1} \cdot (\beta \mathbf{1}) && \rightarrow \text{microdilatation continuum.}
\end{aligned}$$

The microstretch continuum corresponds to

$$\chi = R_\chi \cdot (\beta 1) \tag{22}$$

where β is the scalar microstretch ratio. The micro-gyration tensor $\upsilon = \chi^{\cdot} \cdot \chi^{(-1)}$ then decomposes as

$$\boldsymbol{\upsilon} = \frac{\dot{\beta}}{\beta}\,\mathbf{1} + \boldsymbol{\Omega} \qquad \boldsymbol{\omega} = \operatorname{axial}(\boldsymbol{\Omega}) = -1/2\ \boldsymbol{\epsilon} : \boldsymbol{\Omega} \tag{23}$$

into a spherical part (logarithmic microstretch rate) and a skew-symmetric part Ω (micro-rotation rate) with axial vector ω; here ϵ is the third-order permutation (Levi-Civita) tensor and axial(·) extracts the axial vector of a skew tensor.

Mechanical fields and balance laws

In accordance with the principle of virtual power (Germain, 1973, 2020), the internal virtual power is postulated as (24)

$$P_i = \int_{\mathcal{P}} [\ \mathbf{T} : (\mathbf{L}^* - \boldsymbol{\Omega}^*) + \mathbf{M} : \operatorname{grad}\boldsymbol{\omega}^* + s\left(\operatorname{tr}\mathbf{L}^* - 3\,\frac{\dot{\beta}^*}{\beta}\right) + \mathbf{m} \cdot \operatorname{grad}\left(\frac{\dot{\beta}^*}{\beta}\right)]\, \mathrm{d}v$$

where T is the (in general asymmetric) force-stress tensor, M is the couple-stress tensor, s is the scalar microstretch stress, and m is the microstretch double-stress vector. Applying the divergence theorem and equating with the external virtual power, following the same argument as Section 2.2 with the additional microstructural fields, gives the local balance laws and boundary conditions:

$$\operatorname{div}(\mathbf{T} + s\mathbf{1}) + \mathbf{b}_0 = \mathbf{0} \tag{25}$$

$$\operatorname{div}\mathbf{M} - \boldsymbol{\epsilon} : \mathbf{T} + \mathbf{l}_c = \mathbf{0} \tag{26}$$

$$\operatorname{div}\mathbf{m} + 3s + l_d = 0 \tag{27}$$

$$\mathbf{t} = (\mathbf{T} + s\mathbf{1}) \cdot \mathbf{n} \qquad \mathbf{m}_c = \mathbf{M} \cdot \mathbf{n} \qquad m_d = \mathbf{m} \cdot \mathbf{n} \tag{28}$$

where b_0, l_c, and l_d are the conventional body force, body couple, and microstretch body action, respectively; consistent with the quasi-static setting, no inertial contributions enter. Equation (25) is the balance of linear momentum, (26) the balance of angular momentum, and (27) governs the scalar dilatational degree of freedom.

Free-energy inequality and constitutive equations

The isothermal free-energy inequality for the microstretch continuum is (29)

$$\rho\dot{\psi} - [\quad \mathbf{T}:(\mathbf{L}-\boldsymbol{\Omega}) + \mathbf{M}:\mathrm{grad}\boldsymbol{\omega} + s\left(\mathrm{tr}\mathbf{L} - 3\frac{\dot{\beta}}{\beta}\right) + \mathbf{m}\cdot\mathrm{grad}\left(\frac{\dot{\beta}}{\beta}\right)] \;\le\; 0,$$

For a hyper-elastic microstretch solid, we adopt the objective strain measures (Eringen, 1999; Forest & Sievert, 2006)

$$\mathbf{C} = \mathbf{R}_\chi^T\cdot\mathbf{F} \qquad \boldsymbol{\Gamma} = -1/2\;\boldsymbol{\epsilon}:\left(\mathbf{R}_\chi^T\cdot\mathrm{Grad}\mathbf{R}_\chi\right) \tag{30}$$

$$e = \frac{\det\mathbf{F}}{\det\boldsymbol{\chi}} \qquad \mathbf{K} = \frac{\mathrm{Grad}(\det\boldsymbol{\chi})}{\det\boldsymbol{\chi}} \tag{31}$$

where C is the relative deformation tensor, Γ is the micro-curvature tensor, e is the microstretch-weighted dilatation, and K is the micro-dilatation gradient. With $\psi=\psi(C,\Gamma,e,K)$, the Coleman–Noll procedure (Coleman & Noll, 1974; Hütter, 2020) applied to (29) yields

$$\mathbf{T} = \rho\,\mathbf{R}_\chi\cdot\frac{\partial\psi}{\partial\mathbf{C}}\cdot\mathbf{F}^T \qquad \mathbf{M} = \rho\,\mathbf{R}_\chi\cdot\frac{\partial\psi}{\partial\boldsymbol{\Gamma}}\cdot\mathbf{F}^T \tag{32}$$

$$s = \rho\,e\,\frac{\partial\psi}{\partial e} \qquad \mathbf{m} = \rho\,\frac{\partial\psi}{\partial\mathbf{K}}\cdot\mathbf{F}^T, \tag{33}$$

The rate $\dot{e}/e=\mathrm{tr}L-3\,\dot{\beta}/\beta$, which follows from $\det\chi=\beta^3$, is the microstretch rate conjugate to s in (24). Equations (32)–(33) close the theory for a single-constituent hyper-elastic microstretch continuum.

For small strains and isotropic response, these general relations reduce to the linear microstretch constitutive equations

$$\mathbf{T} = \lambda(\mathrm{tr}\boldsymbol{\varepsilon})\mathbf{1} + 2\mu\,\boldsymbol{\varepsilon}^{sym} + 2\kappa\,\boldsymbol{\varepsilon}^{skw} + b\,e_1\,\mathbf{1} \tag{34}$$

$$\mathbf{M} = \alpha_1\,\boldsymbol{\Gamma} + \alpha_2\,(\mathrm{tr}\boldsymbol{\Gamma})\mathbf{1} + \alpha_3\,\boldsymbol{\Gamma}^T \tag{35}$$

$$s = a\,e_1 + b\,\mathrm{tr}\boldsymbol{\varepsilon} \tag{36}$$

$$\mathbf{m} = c_1\,\mathbf{K} \tag{37}$$

where $\varepsilon=\mathrm{Grad}u-\vartheta\times 1$ is the (generally asymmetric) linear microstretch strain with symmetric part ε^{sym} and skew-symmetric part ε^{skw}, $e_1=\mathrm{Div}u-3\varphi$ is the microstretch dilatation, and ϑ, $\varphi=\beta-1$ are the micro-rotation vector and the scalar microstretch perturbation; $\Gamma=\mathrm{Grad}\vartheta$ and $K=\mathrm{Grad}\varphi$ are the linearized micro-curvature and micro-dilatation gradient. Here λ,μ are the Lamé constants, κ the Cosserat shear modulus, a the microstretch bulk modulus, b the coupling between volumetric macrostrain and microstretch, $\alpha_1,\alpha_2,\alpha_3$ the three isotropic curvature moduli, and c_1 the microstretch-gradient modulus, the nine independent constants of the linear isotropic microstretch continuum, consistent with Eringen's microstretch elasticity (Eringen, 1999). The force stress (34) is asymmetric in general, its skew part $2\kappa\,\varepsilon^{skw}$ measuring the relative rotation between the continuum and its microstructure. The linearization of the strain measures, the isotropic quadratic free energy, and the Coleman–Noll derivation of (34)–(37) are given in Appendix B.

FINDINGS AND DISCUSSION

Microstretch mixture theory

Combining the mixture framework of Section 2 with the microstretch kinematics of Section 3 yields the central object of the paper: a mixture of a microstretch solid skeleton (whose grains may rotate and structurally dilate) and a non-polar pore fluid. Micropolar solid–fluid mixtures (Diebels, 2002) and microstretch mixtures of two solids (Chiriţă & Galeş, 2008) have been formulated before; the contribution here is a mixture that couples a microstretch solid to a non-polar pore fluid within the Theory of Porous Media, derived throughout by the principle of virtual power.

Kinematics of the microstretch mixture

We consider a binary mixture in which only the solid constituent α=s is equipped with microstretch kinematics. The solid micro-deformation tensor is restricted to the microstretch form

$$\chi^{(s)}=R_\chi^{(s)}\cdot(\beta^{(s)}\,1) \tag{38}$$

with micro-gyration tensor decomposed as in (23),

$$\mathbf{v}^{(s)} = \frac{1}{\beta^{(s)}}\frac{d^{(s)}\beta^{(s)}}{dt}\,\mathbf{1} + \mathbf{\Omega}^{(s)} \qquad \boldsymbol{\omega}^{(s)} = \mathrm{axial}\left(\mathbf{\Omega}^{(s)}\right) = -1/2\ \boldsymbol{\epsilon}:\mathbf{\Omega}^{(s)} \tag{39}$$

The fluid constituent α=f is a standard non-polar fluid: it carries only translational kinematics (velocity field $v^{(f)}$ with no independent micro-rotation or microstretch. This is the physically appropriate model for a pore fluid, which has no grain-level rotational or dilatational microstructure.

The scalar microstretch ratio $\beta^{(s)}$ of the solid carries a concrete physical meaning. As the saturating fluid moves into or out of the pore space, the change in local fluid content drives an isotropic rearrangement of the grain-scale structure, an expansion or contraction of the micro-void space at constant grain-material density, rather than a change in the volume of the incompressible mineral grains themselves. This grain-scale structural dilatation is precisely what $\beta^{(s)}$ tracks: it is the microstructural degree of freedom that distinguishes the microstretch mixture from a micropolar mixture, and it provides a kinematic description of the coupling between pore-fluid content and solid microstructure that neither the macroscopic deformation gradient $F^{(s)}$ nor the micro-rotation $R_{\chi}^{(s)}$ can capture alone. The micro-rotation $R_{\chi}^{(s)}$, in turn, records the grain-scale rotation that accompanies non-uniform or shearing deformation of the skeleton: it is inactive under the purely volumetric loading of one-dimensional consolidation, but becomes essential wherever the compaction varies laterally, as in the differential subsidence of Section 5. The two microstructural sectors are thus complementary (dilatation couples to the change in fluid content, rotation to the gradient of the deformation), and the loading determines which is exercised.

Mechanical fields and balance laws

Since only the solid carries microstretch kinematics, the virtual power structure of Section 3.2 applies to the solid constituent with label (s) appended, while the fluid contributes only a translational virtual power. The sole interaction between the two constituents is the linear momentum supply $\mathrm{pl}^{(\alpha)}$. Following Diebels (2002), since the fluid is non-polar it possesses no angular or microstretch DOFs, so the corresponding moment-of-momentum and microstretch-momentum productions acting on the solid from the fluid are set to zero a priori.

For the solid, the internal virtual power extends (24) to

$$P_i^{(s)} = \int_{\mathcal{P}(s)} \Big[\ \mathbf{T}^{(s)}:\left(\mathbf{L}^{*(s)} - \mathbf{\Omega}^{*(s)}\right) + \mathbf{M}^{(s)}:\mathrm{grad}\boldsymbol{\omega}^{*(s)} + s^{(s)}\left(\mathrm{tr}\mathbf{L}^{*(s)} - 3\left(1/\beta^{(s)}\,d^{(s)}\beta^{(s)}/dt\right)^{*}\right) + \mathbf{m}^{(s)}\cdot\mathrm{grad}\left(1/\beta^{(s)}\,d^{(s)}\beta^{(s)}/dt\right)^{*}\Big]\,\mathrm{d}v \tag{40}$$

while the non-polar fluid supplies only the translational internal virtual power

$$P_i^{(f)} = \int_{\mathcal{P}(f)} \mathbf{T}^{(f)} : \mathbf{D}^{*(f)}\ \mathrm{d}v, \tag{41}$$

The divergence theorem, applied together with the balance against the external virtual power (which carries the linear momentum supply $\mathrm{pl}^{(\alpha)}$ for each constituent) yields the local balance laws:

$$\mathrm{div}\left(\mathbf{T}^{(s)} + s^{(s)}\mathbf{1}\right) + \mathbf{b}_0^{(s)} + \mathbf{pl}^{(s)} = \mathbf{0} \tag{42}$$

$$\mathrm{div}\mathbf{M}^{(s)} - \boldsymbol{\epsilon}:\mathbf{T}^{(s)} + \mathbf{l}_c^{(s)} = \mathbf{0} \tag{43}$$

$$\mathrm{div}\mathbf{m}^{(s)} + 3s^{(s)} + l_d^{(s)} = 0 \tag{44}$$

$$\mathrm{div}\mathbf{T}^{(f)} + \mathbf{b}_0^{(f)} + \mathbf{pl}^{(f)} = \mathbf{0} \tag{45}$$

with boundary conditions $t^{(s)}=(T^{(s)}+s^{(s)})\,1)\cdot n$, $m_c^{(s)}=M^{(s)}\cdot n$, $m_d^{(s)}=m^{(s)}\cdot n$, $t^{(f)}=T^{(f)}\cdot n$. Since the fluid has no angular or microstretch DOFs, equations (43) and (44) take the same form as the single-constituent balances of Section 3.2 with label (s): the solid's angular momentum and microstretch momentum are balanced entirely by internal stresses and body actions, with no interaction supply from the fluid.

Invariance of the total mixture virtual power under a superposed rigid-body motion imposes only the linear-momentum constraint

$$\mathrm{pl}^{(s)}+\mathrm{pl}^{(f)}=0. \tag{46}$$

Equation (46) is the mixture-level linear-mo-

mentum balance; no angular- or microstretch-momentum mixture constraints arise because the fluid carries no corresponding DOFs.

Free-energy inequality and constitutive equations
The mixture free-energy inequality for the microstretch solid saturated by the non-polar fluid reduces to (47)

$$\rho^{(s)}\frac{d^{(s)}\psi^{(s)}}{dt}+\rho^{(f)}\frac{d^{(f)}\psi^{(f)}}{dt}$$
$$-\left\{\mathbf{T}^{(s)}:\left(\mathbf{L}^{(s)}-\boldsymbol{\Omega}^{(s)}\right)+\mathbf{M}^{(s)}:\mathrm{grad}\boldsymbol{\omega}^{(s)}\quad+s^{(s)}\left(\mathrm{tr}\mathbf{L}^{(s)}-3\,\frac{1}{\beta^{(s)}}\frac{d^{(s)}\beta^{(s)}}{dt}\right)+\mathbf{m}^{(s)}\right.$$

The single seepage dissipation term $\mathbf{pl}^{(f)}\cdot\mathbf{v}^{(fs)}$ represents the energy dissipated by relative translational flow between the constituents; no angular- or microstretch-momentum exchange terms appear because the fluid carries no corresponding DOFs.

We adopt the solid strain measures (30)–(31) evaluated for the solid phase, with free energies following the constituent-separation principle (Diebels & Ehlers, 1996):

$$\psi^{(s)}=\psi^{(s)}(C^{(s)},\Gamma^{(s)},e^{(s)},K\hat{}^{(s)}),\ \psi^{(f)}=\psi^{(f)}(\rho^{R(f)}). \tag{48}$$

The microstretch $\beta^{(s)}$ describes the grain-scale structural dilatation of the skeleton (the local rearrangement and change of micro-void space) at constant grain-material density; it does not represent compression of the incompressible solid material assumed in Section 2.3, and is therefore an independent, energetically active degree of freedom (Cowin & Nunziato, 1983; Nunziato & Cowin, 1979). Consistent with Section 2.3, the solid free energy $\psi^{(s)}$ does not depend on the volume fraction $n\hat{}^{(s)}$: the grain-scale structural response is carried by the microstretch measures ($e^{(s)}$, $K^{(s)}$), while $n^{(s)}$ remains the kinematic fluid-content variable, so that the energy of the pore space is not counted twice. Applying the Coleman–Noll procedure to (47) yields the solid constitutive equations:

$$\mathbf{T}^{(s)} = \rho^{(s)}\,\mathbf{R}^{(s)}_{\chi}\cdot\frac{\partial\psi^{(s)}}{\partial\mathbf{C}^{(s)}}\cdot\left(\mathbf{F}^{(s)}\right)^{T}-p_{th}\,n^{(s)}\,\mathbf{1} \tag{49}$$
$$\mathbf{M}^{(s)} = \rho^{(s)}\,\mathbf{R}^{(s)}_{\chi}\cdot\frac{\partial\psi^{(s)}}{\partial\boldsymbol{\Gamma}^{(s)}}\cdot\left(\mathbf{F}^{(s)}\right)^{T} \tag{50}$$
$$s^{(s)} = \rho^{(s)}\,e^{(s)}\,\frac{\partial\psi^{(s)}}{\partial e^{(s)}} \tag{51}$$
$$\mathbf{m}^{(s)} = \rho^{(s)}\,\frac{\partial\psi^{(s)}}{\partial\mathbf{K}^{(s)}}\cdot\left(\mathbf{F}^{(s)}\right)^{T} \tag{52}$$

with p_th defined as in (14); as in Section 2.3 no configurational pressure appears, since $\psi^{(s)}$ is independent of $n^{(s)}$. The residual dissipation inequality has the same form as (10) with the solid stress already determined, and yields the fluid split

$$\mathbf{T}^{(f)} = -n^{(f)}\,p_{th}\,\mathbf{1} \tag{53}$$
$$\mathbf{pl}^{(f)Eq} = p_{th}\,\mathrm{grad}n^{(f)} = -\,p_{th}\,\mathrm{grad}n^{(s)} \tag{54}$$
$$\mathbf{pl}^{(f)NEq} = -\mathfrak{B}\cdot\mathbf{v}^{(fs)}$$

B positive semi-definite. The residual inequality admits, in addition, a dissipative equilibrated body force $\pi^{(s)}$ conjugate to the microstretch rate $\beta^{(-1)}\,d^{(s)}\beta/dt$, in the manner of Nunziato and Cowin (1979) and Cowin and Nunziato (1983) and exactly parallel to the way the Darcy drag arises from the seepage dissipation. Requiring the associated dissipation to be non-negative in every process yields the linear law

$$\pi^{(s)} = -\omega^{(s)}\,\frac{1}{\beta^{(s)}}\frac{d^{(s)}\beta^{(s)}}{dt}\qquad \omega^{(s)}\geq 0 \tag{55}$$

with $\omega^{(s)}$ a single new material constant, so that the dissipation is $-\pi^{(s)}(\beta^{(-1)}\,d^{(s)}\beta/dt)=\omega^{(s)}(\beta^{(-1)}\,d^{(s)}\beta/dt)^2\geq 0$. Unlike the force, couple, and microstretch stresses (49)–(52), which remain rate-independent, $\pi\hat{}((s))$ is a dissipative body action: it is the intrinsic (constitutive) part of the microstretch body action $l_d\hat{}((s))$ that the virtual-power balance (44) already carries, identified by the Coleman–Noll split of the residual dissipation exactly as the Darcy drag is the non-equilibrium part of the momentum supply, not a term added to that balance; separating it from the extrinsic part, the balance reads $\mathrm{div}\mathbf{m}^{(s)}+3s^{(s)}+\pi^{(s)}+l_d^{(s)}=0$, and renders it parabolic on linearization (Ap-

pendix C). The rotational sector carries no such term: the micro-rotation is elastically coupled to the macro-rotation through $\kappa^{(s)}$ and is dissipation-free. As in Section 2.3 the pore fluid is inviscid, so its stress is the pure pore pressure and all seepage dissipation is carried by the Darcy drag. Equations (49)–(54) close the microstretch mixture theory: given $\psi^{(s)}$, $\psi^{(f)}$, B, and $\omega^{(s)}$, the field equations (42)–(45) together with these constitutive relations determine the coupled solid motion, microrotation, microstretch, and fluid seepage.

For small strains and isotropic solid response, these reduce to the linear microstretch–poroelastic constitutive equations. The solid stresses are

$$\mathbf{T}^{(s)} = \lambda^{(s)}(\mathrm{tr}\boldsymbol{\varepsilon}^{(s)})\mathbf{1} + 2\mu^{(s)}(\boldsymbol{\varepsilon}^{(s)})^{sym} + 2\kappa^{(s)}(\boldsymbol{\varepsilon}^{(s)})^{skw} + b^{(s)}e_1^{(s)}\mathbf{1} - n_0^{(s)}p_{th}\mathbf{1} \quad (56)$$

$$\mathbf{M}^{(s)} = \alpha_1^{(s)}\boldsymbol{\Gamma}^{(s)} + \alpha_2^{(s)}(\mathrm{tr}\boldsymbol{\Gamma}^{(s)})\mathbf{1} + \alpha_3^{(s)}(\boldsymbol{\Gamma}^{(s)})^T \quad (57)$$

$$s^{(s)} = a^{(s)}e_1^{(s)} + b^{(s)}\mathrm{tr}\boldsymbol{\varepsilon}^{(s)} \quad (58)$$

$$\mathbf{m}^{(s)} = c_1^{(s)}\mathbf{K}^{(s)} \quad (59)$$

and the fluid relations are

$$p_{th} = -\kappa_f \,\mathrm{Div}\mathbf{u}^{(f)} \quad (60)$$

$$\mathbf{T}^{(f)} = -n_0^{(f)}\,p_{th}\,\mathbf{1} \quad (61)$$

$$\mathbf{pl}^{(f)} = p_{th}\,\mathrm{Grad}\tilde{n}^{(s)} - \frac{1}{k}\,\mathbf{v}^{(fs)} \quad (62)$$

where $\varepsilon^{(s)}$ is the linearized (generally asymmetric) solid strain, $e_1^{(s)}$=Divu$^{(s)}$-3$\varphi^{(s)}$ the microstretch dilatation, $\Gamma^{(s)}$ the micro-curvature, $K^{(s)}$ =Grad$\varphi^{(s)}$ the micro-dilatation gradient, $\varphi^{(s)}$=$\beta^{(s)}$ -1 the microstretch perturbation, and $n^{(s)}$ =$n^{(s)}$ -$n_0^{(s)}$. The solid moduli $\lambda^{(s)}$,$\mu^{(s)}$,$\kappa^{(s)}$,$a^{(s)}$,$b^{(s)}$,$\alpha_1^{(s)}$,$\alpha_2^{(s)}$,$\alpha_3^{(s)}$,$c_1^{(s)}$ are those of the microstretch continuum (Appendix B), κ_f is the fluid bulk modulus, $n_0^{(s)}$ the reference solid volume fraction, and k the hydraulic mobility. The solid stress (56) is the microstretch elastic stress augmented by the Biot pore-pressure coupling -$n_0^{(s)}$ p_{th} 1; setting the microstretch moduli to zero recovers the linear Biot–Terzaghi poroelasticity of Section 2.3. The linearization and the Coleman–Noll derivation of (56)–(62) are given in Appendix C.

Special cases: micropolar and microdilatation mixtures

As a consistency check, we verify that the microstretch-mixture field equations reduce to known theories under two restrictions.

Micropolar limit $\beta^{(s)}\equiv1$: Setting $\beta^{(s)}\equiv1$ removes the microstretch degree of freedom identically: $d^{(s)}\,\beta^{(s)}/(dt\,\beta^{(s)})\equiv0$, and $s^{(s)}$, $m^{(s)}$ vanish from (42)–(44). The remaining balance laws reduce to

$$\mathrm{div}\mathbf{T}^{(s)} + \mathbf{b}_0^{(s)} + \mathbf{pl}^{(s)} = \mathbf{0} \quad (63)$$

$$\mathrm{div}\mathbf{M}^{(s)} - \boldsymbol{\epsilon}:\mathbf{T}^{(s)} + \mathbf{l}_c^{(s)} = \mathbf{0} \quad (64)$$

$$\mathrm{div}\mathbf{T}^{(f)} + \mathbf{b}_0^{(f)} + \mathbf{pl}^{(f)} = \mathbf{0} \quad (65)$$

which coincide in structure with the micropolar solid–fluid mixture field equations of (Diebels, 2002), the difference being that Diebels adopts a viscous fluid whereas the present fluid constituent is a non-polar elastic fluid. The strain measures reduce to ($C^{(s)}$,$\Gamma^{(s)}$) with $e^{(s)}\equiv1$, $K^{(s)}\equiv0$, and the constitutive equations (49)–(50) reproduce the micropolar-mixture constitutive structure of (Diebels, 2002; Diebels & Ehlers, 1996), including its linearization as detailed in Appendix C.

Microdilatation limit ($R_\chi^{(s)}\equiv1$): Setting $R_\chi^{(s)}\equiv1$ removes the micro-rotation degree of freedom. The micro-gyration decomposition (39) then gives $\Omega^{(s)}\equiv0$ and $\omega^{(s)}\equiv0$; the micro-curvature $\Gamma^{(s)}$ $\equiv0$ and the couple-stress $M^{(s)}\equiv0$. The angular momentum balance (43) reduces to ϵ:$T^{(s)}$)=$l_c^{(s)}$, which forces the force stress $T^{(s)}$ to be symmetric in the absence of body couples ($l_c^{(s)}$=0).
With $R_\chi^{(s)}\equiv1$ the micro-deformation reduces to $\chi^{(s)}$ =$\beta^{(s)}$ 1, so the relative-deformation measure collapses to the standard right Cauchy–Green tensor

$$C^{(s)} := (F^{(s)})^T F^{(s)} \quad (66)$$

and the solid free energy becomes $\psi^{(s)}$=$\psi^{(s)}$ ($C^{(s)}$,$e^{(s)}$,$K^{(s)}$).
The linear-momentum, microstretch and fluid balances (42), (44) and (45) are unchanged, now with $T^{(s)}$ symmetric. The active strain measures are $C^{(s)}$,$e^{(s)}$,$K^{(s)}$ with $\Gamma^{(s)}\equiv0$. The microstretch constitutive relations (51) and (52) for $s^{(s)}$ and $m^{(s)}$ carry over unchanged, while the force stress

reduces to its symmetric hyperelastic form

$$\mathbf{T}^{(s)} = 2\rho^{(s)}\,\mathbf{F}^{(s)} \cdot \frac{\partial \psi^{(s)}}{\partial \mathbf{C}^{(s)}} \cdot \left(\mathbf{F}^{(s)}\right)^{T} = \left(\mathbf{T}^{(s)}\right)^{T}, \qquad (67)$$

The scalar $\varphi^{(s)} = \beta^{(s)}\text{-}1$ governed by (44) is then the only active microstructural degree of freedom, and this reduced system is the mixture-theoretic analogue of the theory of elastic materials with voids (Cowin & Nunziato, 1983; Nunziato & Cowin, 1979), with $\beta^{(s)}$-1 playing the role of the void-volume fraction; the present formulation extends that theory to a saturated solid–fluid mixture within the TPM framework. With the dissipative body force $\pi^{(s)}$ of (55) retained, this limit is the dissipative microdilatational mixture, in which $\varphi^{(s)}$ relaxes on its own time scale τ_{φ} and one-dimensional consolidation acquires a second, drainage-independent stage.

This microdilatation limit is reached whenever the loading is purely isotropic (irrotational): $\vartheta^{(s)} \equiv 0$ forces $R_{\chi}^{(s)} \equiv 1$, $T^{(s)}$ is symmetric, $C^{(s)} = (F^{(s)})^{T} F^{(s)}$, and the scalar balance (44) governs the dilatational field alone. The differential-subsidence application of Section 5 instead activates both sectors; it recovers this microdilatation limit only where the drawdown is laterally uniform, and otherwise exercises the full microstretch kinematics.

The microstretch mixture theory therefore contains the micropolar-mixture and microdilatation-mixture theories as kinematically consistent special cases, and reduces further to the classical non-polar, non-microstretch binary mixture of Section 2 when both $\beta^{(s)} \equiv 1$ and $R_{\chi}^{(s)} \equiv 1$ are imposed simultaneously.

Application: differential land subsidence and earth-fissure initiation from non-uniform aquifer drawdown

The one-dimensional consolidation of an aquitard under spatially uniform drawdown is purely volumetric: the loading is irrotational, and only the dilatational (microdilatation) sector of the theory is exercised, the microdilatational-mixture limit of Section 4.4. Here we retain the full microstretch mixture and apply it to a loading that activates both microstructural sectors: the differential compaction produced when the aquifer drawdown varies laterally.

Problem statement

Real pumping-induced subsidence is seldom the uniform column of one-dimensional theory. When the head decline varies horizontally (across the edge of a pumped zone, a basin margin, or a buried bedrock step), the aquitard compacts more in some places than in others. The resulting non-uniform, "bowl-shaped" subsidence generates horizontal ground strain, and where that strain is tensile it can open earth fissures: linear tension cracks that are a recognized and damaging geohazard in heavily pumped basins of the US Southwest, the North China Plain, and elsewhere (Holzer & Pampeyan, 1981; Wang et al., 2025; Ye et al., 2018). Field observations associate the fissures with zones of localized differential compaction, near the points of maximum convex-upward curvature of the subsidence profile (Holzer & Pampeyan, 1981).

Two mechanistic pictures coexist in the literature. The classical, tension-based interpretation treats the skeleton as a Cauchy poroelastic continuum and attributes fissures to the horizontal tensile strain at the bowl margin (Holzer & Pampeyan, 1981; Ye et al., 2018). Budhu and Adiyaman (2010) and Budhu (2011) argued instead that the stress state under a laterally declining head carries an antisymmetric part, so that a Cosserat (micropolar) rather than a Cauchy continuum is appropriate, and that fissuring is driven by shear on vertical planes and grain rotation. That analysis, however, is restricted to the soil skeleton under effective stress and omits the pore fluid; a recent case study (Wang et al., 2025) notes explicitly that the fluid mechanics must be included, because the rotation and shear driven by the unbalanced pore pressure may reinforce or oppose those carried by the effective skeletal stress. The present theory supplies exactly this missing ingredient: a satu-

rated mixture in which the grain-scale rotation and dilatation are coupled two-way to the pore fluid, derived consistently from a single variational statement.

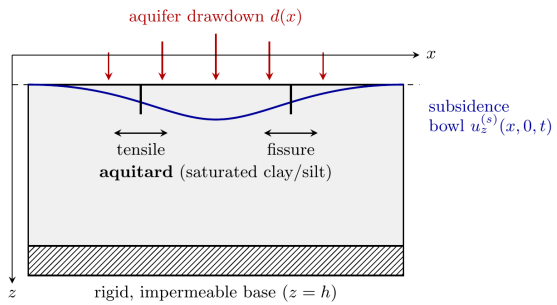


Figure 1: Definition sketch. A saturated aquitard of thickness h in plane strain, drained at the top (z=0) toward a depressurized aquifer whose head declines by a laterally-varying amount d(x) (localized pumping / bedrock step), and bounded below (z=h) by a rigid, impermeable base. Non-uniform drawdown drives differential compaction, a subsidence bowl u_z^((s)) (x,0,t), and a horizontal tensile-strain (earth-fissure) zone at the bowl margin.

We consider the plane-strain section of Figure 1: an aquitard 0≤z≤h, with x horizontal and z vertical, all fields independent of the out-of-plane coordinate. The active solid fields are the displacements $u_x^{(s)}$ (x,z,t), $u_z^{(s)}$ (x,z,t), the out-of-plane micro-rotation angle $\vartheta^{(s)}$ (x,z,t) (the single in-plane-active component of the linearized micro-rotation vector $\vartheta^{(s)}$ of Appendix B, written non-bold; it is a rotation angle, not the micro-rotation rate $\omega^{(s)}$ of Section 3.1), and the microdilatation $\varphi^{(s)}$ (x,z,t); the fluid field is the pore pressure p_{th} (x,z,t). The essential kinematic point is that a laterally-varying subsidence carries a non-zero macro-rotation, (68)

$$\Theta = 1/2\,(\partial_z u_x^{(s)} - \partial_x u_z^{(s)}) \neq 0 \text{ "whenever" } \partial_x u_z^{(s)} \neq 0,$$

together with the volumetric compaction $\varepsilon = \partial_x u_x^{(s)} + \partial_z u_z^{(s)} \neq 0$. Both microstructural sectors are therefore active, in contrast to the uniform-drawdown (one-dimensional) case, in which $\partial_x(\cdot) \equiv 0$, $\Theta \equiv 0$, and only $\varphi^{(s)}$ survives.

Governing equations in plane strain

We adopt the consolidation simplifications of Section 2.3: incompressible solid grains and the incompressible-fluid limit ($\kappa_f \to \infty$) of the barotropic pore fluid, in which the pore pressure is no longer given by (14) and its linearization but becomes the reaction to the saturation constraint, determined by the fluid mass balance (76) below, with the fluid partial stress reducing to that pressure and seepage resisted by Darcy drag, and quasi-static deformation. Specializing the linear microstretch–poroelastic constitutive equations (56)–(62) to plane strain, the in-plane Cartesian components $T_{ij}^{(s)}$ of the solid partial stress $T^{(s)}$ are as follows. Throughout this section $T_{ij}^{(s)}$ denotes the stress on the face of outward normal e_i acting in the direction e_j, so that the force balances (72)–(73) below read $\partial_i T_{ij}^{(s)} = 0$; this is the transpose of the component ordering implied by the stress power T:L of Section 3.2, and in it the angular-momentum balance (43) reduces to the screened moment balance (74) with the skew stress (71) exactly as written (the sign of (71) is tied to this ordering and reverses under the transpose). The components are

$$T_{xx}^{(s)} = \lambda^{(s)}\varepsilon + 2\mu^{(s)}\,\partial_x u_x^{(s)} + b^{(s)} e_1 - n_0^{(s)} p_{th} \quad (69)$$

$$T_{zz}^{(s)} = \lambda^{(s)}\varepsilon + 2\mu^{(s)}\,\partial_z u_z^{(s)} + b^{(s)} e_1 - n_0^{(s)} p_{th} \quad (70)$$

while the shear stresses are asymmetric, their skew part measuring the relative rotation between continuum and grains,

$$T_{xz}^{(s)} - T_{zx}^{(s)} = 4\kappa^{(s)}\,(\vartheta^{(s)} - \Theta), \quad (71)$$

with $\varepsilon \equiv \mathrm{Div} u^{(s)} = \mathrm{tr}\varepsilon^{(s)}$ the volumetric strain, $e_1 = \varepsilon - 3\varphi^{(s)}$ the microdilatation strain, $s^{(s)} = a^{(s)} e_1 + b^{(s)}\,\varepsilon$ the scalar microdilatation stress of (58), and $\kappa^{(s)}$ the Cosserat modulus. The couple stress $M^{(s)}$ carries the plane-strain components $\gamma^{(s)}\,\mathrm{grad}\vartheta^{(s)}$, and the microdilatation double-stress is $m^{(s)} = c_1^{(s)}\,\mathrm{grad}\varphi^{(s)}$, where $\gamma^{(s)}$ is the effective plane-strain curvature modulus. In plane strain the micro-rotation reduces to the single out-of-plane scalar $\vartheta^{(s)}$, so the linearized micro-curvature $\Gamma^{(s)} = \mathrm{Grad}\vartheta^{(s)}$ of (57) retains only the two

components $\partial_x \vartheta^{(s)}$ and $\partial_z \vartheta^{(s)}$; its isotropic invariants collapse to $\Gamma^{(s)}:\Gamma^{(s)}=|\mathrm{grad}\vartheta^{(s)}|^2$, $\mathrm{tr}\Gamma^{(s)}=0$ and $\Gamma^{(s)}:(\Gamma^{(s)})^{T}=0$, so the three curvature moduli of (57) reduce to $\alpha_1^{(s)}$ alone and $\gamma^{(s)}=\alpha 1^{(s)}$. The quasi-static balance laws (42)–(45) then reduce to the coupled system

$$\partial_x\left(T_{xx}^{(s)}+s^{(s)}\right)+\partial_z T_{zx}^{(s)} = 0 \quad (72)$$

$$\partial_x T_{xz}^{(s)}+\partial_z\left(T_{zz}^{(s)}+s^{(s)}\right) = 0 \quad (73)$$

$$\gamma^{(s)}\nabla^2\vartheta^{(s)}-4\kappa^{(s)}\vartheta^{(s)}+4\kappa^{(s)}\Theta = 0 \quad (74)$$

$$c_1^{(s)}\nabla^2\varphi^{(s)}-9a^{(s)}\varphi^{(s)}+3\left(a^{(s)}+b^{(s)}\right)\varepsilon = 0 \quad (75)$$

closed by the fluid mass balance for incompressible constituents,

$$\partial_t \varepsilon = k\nabla^2 p_{th}, \quad (76)$$

in which k is the hydraulic mobility and $\nabla^2=\partial_{xx}+\partial_{zz}$. Equations (72)–(76) govern the five fields $(u_x^{(s)},u_z^{(s)},\vartheta^{(s)},\varphi^{(s)},p_{th})$. The moment balance (74) is a screened-Helmholtz equation for $\vartheta^{(s)}$ whose source is the macro-rotation angle Θ of (68) (half the curl of $u^{(s)}$; distinct from the micro-gyration tensor $\Omega^{(s)}$ of Section 3.1); the isotropic microdilatation stress $s^{(s)}$ enters the force balances (72)–(73) through the term $s^{(s)}$ 1 of (42); the microdilatation balance (75) is $\mathrm{div}m^{(s)}+3s^{(s)}=0$, the equilibrated (elliptic) form of the voids balance. The dissipative equilibrated body force $\pi^{(s)}$ of (55) makes the full voids balance parabolic, (94), with relaxation time $\tau_\varphi=\omega^{(s)}/9a^{(s)}$; the present analysis adopts the fast-relaxation regime $\tau_\varphi \ll t_c$, in which the grain-scale dilatation equilibrates with the deformation on the consolidation time scale and the fluid balance (76) alone carries the time-dependence. The finite-τ_φ response of the dilatational sector, which under laterally uniform drawdown produces a delayed secondary compression, is a one-dimensional effect outside the scope of this fissure-oriented study.

The boundary conditions are, at the drained top z=0, vanishing total traction (the vertical traction carrying the isotropic microstretch stress $s^{(s)}$ as in (73), and the fluid partial stress being $-(1-n_0^{(s)})p_{th}$ 1) together with the imposed pore-pressure decline,

$$T_{zz}^{(s)}+s^{(s)}-(1-n_0^{(s)})\,p_{th}=0,\ T_{zx}^{(s)}=0,\ \partial_z\vartheta^{(s)})=0,\ \partial_z\varphi^{(s)}=0,\ p_{th}=-d(x), \quad (77)$$

and a rigid, impermeable base at z=h,

$$u_x^{(s)}=u_z^{(s)}=0,\ \vartheta^{(s)}=0,\ \partial_z\varphi^{(s)}=0,\ \partial_z p_{th}=0. \quad (78)$$

The non-uniform drawdown enters as the laterally-varying pore-pressure decline $p_{th}=-d(x)$ imposed at t=0 at the drained boundary, with the total overburden traction unchanged, so that the interior pressure starts from zero and the decline diffuses into the layer; the effective vertical stress at the boundary rises by d(x) at once. In one dimension this loading is exactly equivalent to the classical Terzaghi step of vertical effective stress d applied at the surface (the two give identical compaction histories). In two dimensions it is not: the two total-stress fields differ by the isotropic field -d(x)1, whose divergence -d'(x) e_x is a horizontal force acting precisely where the drawdown varies, so the surface-load problem over-predicts both the subsidence and the fissure strain for a pumping-induced drawdown. We therefore impose the pore-pressure decline directly.

Internal length scales and the microdilatational limit

The system carries two internal length scales and one time scale. The moment balance (74) regularizes the micro-rotation over the Cosserat length

$$\ell_c = \sqrt{\gamma^{(s)}/4\kappa^{(s)}} \quad (79)$$

the voids balance (75) regularizes $\varphi^{(s)}$ over the microdilatation length $l_v=\sqrt{c_1^{(s)}/9a^{(s)}}$, and the fluid balance (76) sets the consolidation time $t_c=h^2/c_v$, $c_v=k(\lambda^{(s)}+2\mu^{(s)})$. Because the coefficients are independent of x, each horizontal Fourier mode $\propto e^{iqx}$ evolves independently: the two-dimensional problem reduces to a coupled system

of ordinary differential equations in z for each wavenumber q, advanced in time and synthesized over q to represent an arbitrary drawdown pattern d(x).

The wavenumber q measures the sharpness of the lateral drawdown gradient and acts as the control that switches the rotation sector on. In the source of (74), the macro-rotation of a laterally-varying subsidence is $2\Theta=\partial_z u_x^{(s)}-\partial_x u_z^{(s)}$, whose dominant part $\partial_x u_z^{(s)}\sim iq\,\hat{u}_z^{(s)}$ is the horizontal variation of vertical displacement (differential subsidence itself) and carries an explicit factor of q. As $q\to0$ (spatially uniform drawdown) this source vanishes, (74) gives $\vartheta^{(s)}\to0$, the force stress becomes symmetric, and the horizontal/rotational fields decouple from the loading; the remaining vertical fields $u_z^{(s)},\varphi^{(s)},p_{th}$ satisfy exactly the one-dimensional parabolic–elliptic consolidation system of the microdilatational-mixture limit (in the fast-relaxation regime $\tau_\varphi\ll t_c$ adopted here), in which the grain-scale dilatation relaxes the drained stiffness and reduces the effective consolidation coefficient below the classical Terzaghi value. The microdilatational mixture of Section 4.4 is therefore recovered precisely as the uniform-drawdown ($q\to0$) limit of the present theory: the microstretch mixture contains it as a structural special case, not merely by analogy.

Results: regularization and temporal evolution of the fissure zone

We solve (72)–(76) for a localized drawdown $d(x)=\Delta p_0\exp(-x^2/2\sigma^2)$ representing a pumped-zone edge of lateral extent $\sigma=0.15h$, with $\nu=1/4$ and illustrative, uncalibrated microdilatation moduli $a^{(s)}=0.5\,M_0$, $b^{(s)}=0.3\,M_0$, $l_v=0.1h$ ($M_0=\lambda^{(s)}+2\mu^{(s)}$, varying the Cosserat length l_c at fixed coupling number $N_c^2=2\kappa^{(s)}/(\mu^{(s)}+\kappa^{(s)})=1/2$, Eringen's coupling number written in the moduli of (56) (i.e. $\kappa^{(s)}=\mu^{(s)}/3$). The classical reference is the Cauchy material $\kappa^{(s)}=0$ with the same $\lambda^{(s)}$, $\mu^{(s)}$. Because $\kappa^{(s)}$ multiplies only the skew strain in (56), this is exactly the limit $l_c\to0$ of the Cosserat material, in which the micro-rotation locks to the macro-rotation; we verified numerically that the two solutions agree to 0.5% at 81 nodes, 0.2% at 161 and 0.1% at 321, the difference halving with each refinement, so the comparison isolates the length-scale effect at fixed drained moduli. The Cosserat length of a granular skeleton is of the order of the grain diameter (Mühlhaus & Vardoulakis, 1987), and shear bands are a few tens of grain diameters thick; for the silt and clay of an aquitard h=20–50 m thick this places the grain and shear-band scales at $l_c/h\lesssim10^{(-3)}$–$10^{(-2)}$. We therefore treat l_c as a structural (fabric or meso-scale) length of the skeleton to be identified from field records, and read the values l_c=0.15h and 0.3h as the mechanism's upper bound rather than as estimates; for l_c=0.3h the length also exceeds the load width $\sigma=0.15h$, so part of the reduction there is a size effect of the narrow load. The width $\sigma=0.15h$ is itself an idealization: pumping cones are kilometers wide, and the sharp lateral compaction gradients that fissure a basin arise from its geology (a bedrock step or an abrupt change of aquitard thickness); the narrow d(x) stands in for such a gradient and the results should be read in that light. Time is measured in units of t_c, and horizontal strains in units of the natural consolidation strain $\Delta p_0/M_0$. Each horizontal Fourier mode is integrated in z by a second-order finite-difference scheme (81 nodes) and advanced in time by implicit Euler, and the surface fields are synthesized over modes; the results are insensitive to further mesh and time-step refinement. Figure 2 summarizes the response.(Fig. 2)

Differential compaction produces a subsidence bowl that deepens over the consolidation time (Fig. 2a) and, at its margin, a concentration of horizontal tensile strain, the earth-fissure zone (Fig. 2b). Two results are central. First, the Cosserat length regularizes the fissure zone: the classical limit ($l_c\to0$) gives the sharpest and most intense strain concentration, whereas a finite l_c caps the peak tensile strain and, in place of that sharp concentration, spreads it over a zone of finite width. The effect is set by l_c/h. At

the structural scale l_c=$10^{(-2)}$ h the response is the classical one: its difference from $\kappa^{(s)}$=0 is 0.4% at 81 nodes and halves with each grid refinement, i.e. it is discretization error, and the curve is indistinguishable from the classical one in Fig. 2b,c (l_c=$10^{(-3)}$ h gives the same). The regularization becomes significant only when l_c is a sizeable fraction of the layer thickness: over l_c:$10^{(-2)}$ h→0.3h the peak fissure-driving strain at full consolidation falls to about 70% of the classical value, with 86% at l_c=0.15h, and the tensile zone broadens by about one-sixth (its half-maximum width growing from 1.4h to 1.6h). Second, the fissure zone evolves in time (Fig. 2c): because the pressure decline diffuses in from the boundary, the peak tensile strain rises within the first few percent of the consolidation time to about 1.6 times its final value, while the pore-pressure gradients are steepest near the drainage boundary, and then relaxes to the lower steady value as consolidation completes. Where the reduction is present it is present at every instant, and it is strongest in that early stage (the l_c=0.3h peak is about half the classical one at t/t_c=0.02, seven-tenths at full consolidation), because the Cosserat length acts on the sharp early strain gradients.

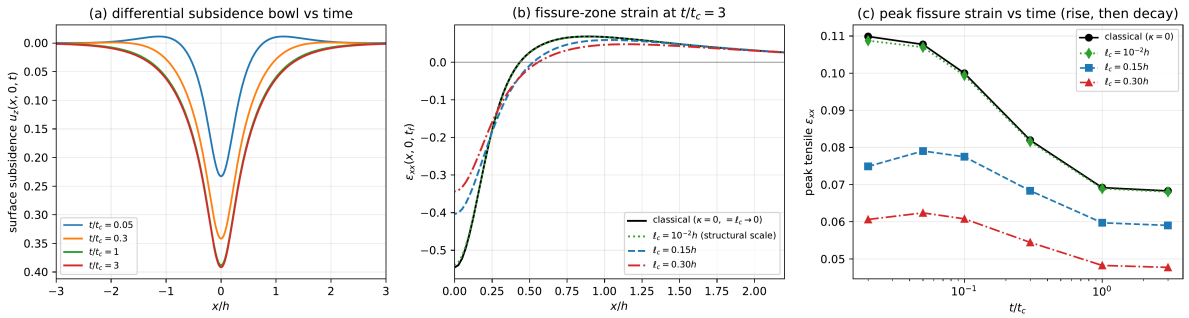


Figure 2: Differential subsidence and fissure-zone response to a localized drawdown. (a) The subsidence bowl $u_z^{(s)}$ (x,0,t) deepens over the consolidation time. (b) Surface horizontal strain ε_{xx} (x,0) at full consolidation: the classical limit (l_c→0 of the same material) gives a sharp, intense tensile concentration at the bowl margin; at the structural scale l_c=$10^{(-2)}$ h the response is indistinguishable from it, while l_c=0.15h and 0.3h cap and widen the peak. (c) The peak tensile (fissure-driving) strain rises within the first few percent of t_c as the pressure decline penetrates the layer, then relaxes to its steady value; it is reduced at every instant for the larger Cosserat lengths, most strongly in the early stage.

Implications for earth-fissure hazard

These results carry three testable consequences. First, classical Cauchy poroelasticity over-predicts the peak horizontal strain that a fissure-initiation threshold would be compared against; the microstretch theory replaces the sharp classical strain concentration with a lower, broader peak whose value depends on l_c. Fissure-hazard assessments based on a classical strain criterion are therefore conservative by an amount set by l_c/h: negligible at the grain and shear-band scales, and substantial only if the skeleton carries a structural length a sizeable fraction of the layer thickness, which is an empirical question the l_c-dependence makes testable. Second, the fissure zone acquires a finite width that broadens with the microstretch length scales, comparable to the finite width of observed fissure zones and to horizontal-strain profiles retrieved from InSAR (Wang et al., 2025; Ye et al., 2018). Third, because the peak strain is largest early in the consolidation and relaxes as it completes, the theory predicts that fissure risk is greatest shortly after the head decline, diminishing as the layer drains, a temporal signature that lumped, time-independent stress analyses cannot produce.

The model also reconciles the two mechanis-

tic pictures of fissuring. It carries both the tensile/dilatational mechanism (through $\varphi^{(s)}$) and ε, following the classical view (Holzer & Pampeyan, 1981)) and the shear/rotation mechanism (through $\vartheta^{(s)}$) and the antisymmetric stress (71), following Budhu and Adiyaman (2010) and Budhu (2011)) within one thermodynamically consistent, fluid-coupled framework, and quantifies their competition as the pore pressure evolves, the coupling that (Wang et al., 2025) identified as missing from the dry Cosserat analysis. Calibration of the Cosserat and microdilatation moduli against extensometer, leveling, and InSAR records, and the resulting discrimination between the rotation- and tension-dominated regimes, are natural directions for future work.

RESULTS AND CONCLUSION

This paper has set out a microstretch mixture theory for a saturated porous medium, a microstretch solid skeleton interpenetrated by a non-polar elastic fluid, with the balance laws obtained from the principle of virtual power and the constitutive equations closed by the Coleman–Noll procedure in the Theory of Porous Media. The theory adds grain-scale rotation and dilatation to classical poroelasticity, coupled two-way to the pore fluid, and reduces exactly to Biot–Terzaghi poroelasticity, and to the micropolar- and microdilatation-mixture theories, in the appropriate limits. What it adds is a consistent passage from one variational statement to a closed, thermodynamically admissible set of field and constitutive equations in which both grain-scale mechanisms are retained.

Applied to the differential compaction of an aquitard under laterally non-uniform drawdown, the theory activates both microstructural sectors and yields a result absent from classical poroelasticity: a Cosserat length scale of the skeleton regularizes the earth-fissure zone. Classical Cauchy poroelasticity predicts a sharp horizontal-strain concentration at the subsidence-bowl margin; the microstretch Cosserat length caps this peak (to roughly seven-tenths of the classical value when the length is three-tenths of the layer thickness, the mechanism's upper bound; at the grain and shear-band scales the correction vanishes and the classical prediction is recovered) and spreads it over a fissure zone of finite width. Because the fissure-driving strain develops in time with consolidation and is largest early, shortly after the head decline, the theory predicts that fissure risk is greatest at that stage and diminishes as the layer drains. For spatially uniform drawdown the rotation sector switches off and the response reduces exactly to the one-dimensional microdilatational-mixture consolidation of Section 4.4. The framework carries both the tensile/dilatational and the shear/rotation mechanisms of earth fissuring within one thermodynamically consistent, fluid-coupled theory, and quantifies their competition as the pore pressure evolves. Its testable predictions (a fissure zone broadened and regularized by the Cosserat length, a reduced peak strain, and fissure risk concentrated early in the consolidation) distinguish it from both classical poroelastic and dry-Cosserat models; their calibration against extensometer, leveling, and InSAR records is left for future work.

Several extensions are natural. Mass exchange between the constituents has been excluded; a mass-supply term in (5) would open the theory to reactive or phase-changing mixtures. The constitutive relations are isotropic and hyper-elastic; anisotropy of the microstretch response, or a fluid endowed with microstructure of its own, would widen the class of materials covered. The analysis of Section 5 is quasi-static and assumes an incompressible fluid; reinstating the inertial and micro-inertial terms would yield the corresponding dynamic theory, a distinct line of work. These directions, together with the calibration of the Cosserat length $l_c=\sqrt{\alpha_1^{(s)}/4\kappa^{(s)}}$ and the microdilatation length $l_v=\sqrt{c_1^{(s)}/9a^{(s)}}$ against field records, define a program for developing the theory toward quantitative prediction of pumping-induced ground failure.

REFERENCES

Atkin, R. J., & Craine, R. E. (1976). Continuum theories of mixtures: Basic theory and historical development. The Quarterly Journal of Mechanics and Applied Mathematics, 29(2), 209–244. https://doi.org/10.1093/qjmam/29.2.209

Bedford, A., & Drumheller, D. S. (1983). Theories of immiscible and structured mixtures. International Journal of Engineering Science, 21(8), 863–960. https://doi.org/10.1016/0020-7225(83)90071-X

Biot, M. A. (1941). General theory of three-dimensional consolidation. Journal of Applied Physics, 12(2), 155–164. https://doi.org/10.1063/1.1712886

Bowen, R. M. (1976). Theory of mixtures. In A. C. Eringen (Ed.), Continuum physics (Vol. 3, pp. 1–127). Academic Press.

Bowen, R. M. (1980). Incompressible porous media models by use of the theory of mixtures. International Journal of Engineering Science, 18(9), 1129–1148.

Bowen, R. M. (1982). Compressible porous media models by use of the theory of mixtures. International Journal of Engineering Science, 20(6), 697–735.

Budhu, M. (2011). Earth fissure formation from the mechanics of groundwater pumping. International Journal of Geomechanics, 11(1), 1–11. https://doi.org/10.1061/(ASCE)GM.1943-5622.0000060

Budhu, M., & Adiyaman, I. B. (2010). Mechanics of land subsidence due to groundwater pumping. International Journal for Numerical and Analytical Methods in Geomechanics, 34(14), 1459–1478. https://doi.org/10.1002/nag.863

Chiriţă, S., & Galeş, C. (2008). A mixture theory for microstretch thermoviscoelastic solids. Journal of Thermal Stresses, 31(11), 1099–1124.

Coleman, B. D., & Noll, W. (1974). The thermodynamics of elastic materials with heat conduction and viscosity. In W. Noll, The foundations of mechanics and thermodynamics: Selected papers. Springer. https://doi.org/10.1007/978-3-642-65817-4 (Reprinted from Archive for Rational Mechanics and Analysis, 13, 167–178, 1963)

Cowin, S. C., & Nunziato, J. W. (1983). Linear elastic materials with voids. Journal of Elasticity, 13(2), 125–147. https://doi.org/10.1007/BF00041230

dell'Isola, F., & Placidi, L. (2011). Variational principles are a powerful tool also for formulating field theories. In F. dell'Isola & S. Gavrilyuk (Eds.), Variational models and methods in solid and fluid mechanics (CISM International Centre for Mechanical Sciences, Vol. 535). Springer. https://doi.org/10.1007/978-3-7091-0983-0_1

Del Piero, G. (2009). On the method of virtual power in continuum mechanics. Journal of Mechanics of Materials and Structures, 4(2), 281–292. https://doi.org/10.2140/jomms.2009.4.281

Diebels, S. (2001). Evolution of the volume fractions in compressible porous media. In W. Ehlers (Ed.), IUTAM Symposium on Theoretical and Numerical Methods in Continuum Mechanics of Porous Materials (Solid Mechanics and Its Applications, Vol. 87). Springer. https://doi.org/10.1007/0-306-46953-7_3

Diebels, S. (2002). Micropolar mixture models on the basis of the Theory of Porous Media. In W. Ehlers & J. Bluhm (Eds.), Porous media: Theory, experiments and numerical applications (pp. 121–145). Springer. https://doi.org/10.1007/978-3-662-04999-0_3

Diebels, S., & Ehlers, W. (1996). On fundamental concepts of multiphase micropolar materials. Technische Mechanik, 16(1), 77–88.

Ehlers, W. (2002). Foundations of multiphasic and porous materials. In W. Ehlers & J. Bluhm (Eds.), Porous media: Theory, experiments and numerical applications (pp. 3–86). Springer. https://doi.org/10.1007/978-3-662-04999-0_1

Eringen, A. C. (1999). Microcontinuum field theories: I. Foundations and solids. Springer. https://doi.org/10.1007/978-1-4612-0555-5

Forest, S., & Sievert, R. (2006). Nonlinear microstrain theories. International Journal of Solids and Structures, 43(24), 7224–7245. https://doi.org/10.1016/j.ijsolstr.2006.05.012

Galloway, D. L., & Burbey, T. J. (2011). Review: Regional land subsidence accompanying groundwater extraction. Hydrogeology Journal, 19(8), 1459–1486. https://doi.org/10.1007/s10040-011-0775-5

Germain, P. (1973). The method of virtual power in continuum mechanics. Part 2: Microstructure. SIAM Journal on Applied Mathematics, 25(3), 556–575. https://doi.org/10.1137/0125053

Germain, P. (2020). The method of virtual power in the mechanics of continuous media, I: Second-gradient theory. Mathematics and Mechanics of Complex Systems, 8(2), 153–190. https://doi.org/10.2140/memocs.2020.8.153

Green, A. E., & Rivlin, R. S. (1964). On Cauchy's equations of motion. Zeitschrift für angewandte Mathematik und Physik, 15, 290–292. https://doi.org/10.1007/BF01607019

Hassanizadeh, M., & Gray, W. G. (1979a). General conservation equations for multi-phase systems: 1. Averaging procedure. Advances in Water Resources, 2, 131–144. https://doi.org/10.1016/0309-1708(79)90025-3

Hassanizadeh, M., & Gray, W. G. (1979b). General conservation equations for multi-phase systems: 2. Mass, momenta, energy, and entropy equations. Advances in Water Resources, 2, 191–203.

Holzer, T. L., & Pampeyan, E. H. (1981). Earth fissures and localized differential subsidence. Water Resources Research, 17(1), 223–227. https://doi.org/10.1029/WR017i001p00223

Hütter, G. (2020). Coleman–Noll procedure for classical and generalized continuum theories. In H. Altenbach & A. Öchsner (Eds.), Encyclopedia of continuum mechanics (pp. 316–323). Springer.

Mariano, P. M. (2016). Trends and challenges in the mechanics of complex materials: A view. Philosophical Transactions of the Royal Society A: Mathematical, Physical and Engineering Sciences, 374, 20150341. https://doi.org/10.1098/rsta.2015.0341

Maugin, G. A. (2017). Non-classical continuum mechanics: A dictionary (Advanced Structured Materials, Vol. 51). Springer. https://doi.org/10.1007/978-981-10-2434-4

Mindlin, R. D. (1964). Micro-structure in linear elasticity. Archive for Rational Mechanics and Analysis, 16(1), 51–78. https://doi.org/10.1007/BF00248490

Mühlhaus, H.-B., & Vardoulakis, I. (1987). The thickness of shear bands in granular materials. Géotechnique, 37(3), 271–283. https://doi.org/10.1680/geot.1987.37.3.271

Noll, W. (1974). La mécanique classique, basée sur un axiome d'objectivité. In The foundations of mechanics and thermodynamics: Selected papers. Springer. https://doi.org/10.1007/978-3-642-65817-4

Nunziato, J. W., & Cowin, S. C. (1979). A nonlinear theory of elastic materials with voids. Archive for Rational Mechanics and Analysis, 72(2), 175–201. https://doi.org/10.1007/BF00249363

Poland, J. F. (Ed.). (1984). Guidebook to studies of land subsidence due to ground-water withdrawal (Studies and Reports in Hydrology, Vol. 40). UNESCO.

Quiligotti, S., Maugin, G. A., & dell'Isola, F. (2003). An Eshelbian approach to the nonlinear mechanics of constrained solid–fluid mixtures. Acta Mechanica, 160(1–2), 45–60. https://doi.org/10.1007/s00707-002-0968-z

Terzaghi, K. (1943). Theoretical soil mechanics. John Wiley & Sons. https://doi.org/10.1002/9780470172766

Truesdell, C. (1984). Thermodynamics of diffusion. In Rational thermodynamics (2nd ed.). Springer. https://doi.org/10.1007/978-1-4612-5206-1

Twiss, R. J., & Eringen, A. C. (1971). Theory of mixtures for micromorphic materials—I: Balance laws. International Journal of Engineering Science, 9(10), 1019–1044.

Wang, G.-Y., Zhu, J.-Q., You, G. G., Zhang, D., Yu, J., Gou, F.-G., & Wu, J.-Q. (2025). Earth fissures during groundwater depletion and recovery: A case study at Shitangwan, Wuxi, Jiangsu, China. Hydrology, 12(3), 62. https://doi.org/10.3390/hydrology12030062

Ye, S., Franceschini, A., Zhang, Y., Janna, C., Gong, X., Yu, J., & Teatini, P. (2018). A novel approach to model earth fissure caused by extensive aquifer exploitation and its application to the Wuxi case, China. Water Resources Research, 54(3), 2249–2269. https://doi.org/10.1002/2017WR021872

COPYRIGHTS
©2023 The author(s). This is an open access article distributed under the terms of the Creative Commons Attribution (CC BY 4.0), which permits unrestricted use, distribution, and reproduction in any medium, as long as the original authors and source are cited. No permission is required from the authors or the publishers.

HOW TO CITE THIS ARTICLE
Ghiasi tarzi, A., Robati, A. & Kazerooni sadi, M. A. (2026). A Microstretch Mixture Theory for Differential Land Subsidence and Earth-Fissure Initiation from Non-uniform Aquifer Drawdown. (e743954). International Journal of Urban Management and Energy Sustainability, 7(2), e743954
DOI:10.22034/ijumes.2026.2110389.1432